Iterative cluster expansion approach for predicting the structure evolution of mixed Ruddelsden-Popper oxides $La_{2-x}Sr_xNi_{1-y}Fe_yO_{4\pm\delta}$

Debalaya Sarker,[1,2,*,†] Zhong-Kang Han,[2,3,*] and Sergey V. Levchenko[2,‡]
[1]UGC-DAE Consortium for Scientific Research Indore, Khandwa Road, Indore 452001, India
[2]Center for Energy Science and Technology, Skolkovo Institute of Science and Technology, Moscow 121205, Russia
[3]School of Materials Science and Engineering, Zhejiang University, Hangzhou 310058, China

(Received 1 October 2022; revised 10 March 2023; accepted 9 May 2023; published 31 May 2023)

Layered perovskites viz. Ruddlesden-Popper (RP) compounds have attracted a significant research interest lately due to their superior electrocatalytic activities, on top of their rich physics. Although the versatility of their compositional space is the key to tune their stability and applicability, its complexity also makes the understanding and design of new functional RP-based materials difficult. Herein by parameterizing a cluster expansion model Hamiltonian with density-functional inputs, we have successfully scanned over the complex configurational space of an RP phase, taking $La_{2-x}Sr_xNi_{1-y}Fe_yO_{4\pm\delta}$ as an example. This surrogate model is then used to predict the energies of unknown compositions and performing Metropolis Monte Carlo sampling for finding the ground-state structures. By analyzing these stable configurations at different x, y's, and δ=0, 0.125, we found that apical vacancies in the rock-salt layer are more favorable due to lesser steric forces but changes in A-site oxidation state due to Sr substitution can facilitate equatorial O-vacancy formation even in the perovskite layers. Our results uncover the structural evolution of RP oxides with increasing A-site (Sr) and B-site (Fe) substitutions. We find that a critical Sr concentration is required to stabilize Fe in these systems. With increasing Sr concentration, the A-site charge state changes gradually from La^{+3} to Sr^{+2}, which facilitates both O-vacancy formation and stabilization of the B-site dopants. The findings further highlight the effects of configurational changes for the same composition on electronic structure. Thus, our work clearly demonstrates the importance of exploring configurational space of these complex oxides when using electronic-structure features as descriptors of their catalytic and other functional properties.

DOI: 10.1103/PhysRevMaterials.7.055802

I. INTRODUCTION

Layered perovskites viz. Ruddlesden-Popper (RP) phases ($A_{2-x}A'_xB_{1-y}B'_yO_{4\pm\delta}$, where A is a rare-earth, alkaline, or alkaline-earth element, and B is a transition metal) are emerging electrocatalysts, which have been demonstrated to have an immense potential for several applications, in particular, as electrocatalysts for the oxygen evolution reaction and small organic molecule oxidation [1]. The substitution at either A-site or B-site provides means for versatile tuning of physical properties in this class of materials. For example, in La_2NiO_4, coexistence of Ni and Fe at the B/B' sites results in enhanced mass activity for urea oxidation. Coexisting orthorhombic and tetragonal phases in Ba-doped layered La cuprates have been held responsible for suppression of superconductivity around 1/8th-doping concentrations, which were otherwise attributed to charge-density waves ordering in the low-temperature tetragonal phase [2]. Also, the nature and direction of charge ordering gets modified with the nature of B-site transition metals: while charge ordering along the (1,0) direction of the CuO_2 square plane are favored in the cuprates, the diagonal charge stripes along the (1,1) direction of the NiO_2 plane are stable in the Sr-doped double-layered La nickelates. Interestingly, the RP phase can accomodate even larger variety of metal cations while preserving stability as compared to the perovskite phase, also known for its versatility.

With the increasing interest in applications of both A- and B-site-doped RP oxides, many experimental and computational studies have been carried out to unravel the structure-property relations in La-based RP oxides. The O-2p band center was shown to be a descriptor for oxygen evolution reaction (OER) activity by Xie *et al.* [3] for $(La_{1-x}Sr_x)_2MO_{4\pm\delta}$ (with M = Co, Ni, and Cu) RP oxides. On the other hand, activity towards urea oxidation has been directly correlated to the number of Ni-O-Fe bonds by Forslund *et al.* [1]. However, in all these studies, a certain arrangement of the dopants was assumed, often based simply on the convenience of calculations. Also, the thermodynamic stability of the system would be largely dependent not only on the distribution of oxygen vacancies/interstitials, but also on the arrangement of A/A' and B/B' sites. Thus, exploring the phase space of these materials at realistic conditions is the first crucial step towards understanding their properties and rational design of new and improved functional materials for targeted applications at certain environmental conditions.

As the understanding of vacancy/substitutional defect-mediated electronic structure is crucial for improved property predictions, finding the correct ground state is, therefore,

*These authors contributed equally to this work.
†debalaya@csr.res.in
‡s.levchenko@skoltech.ru

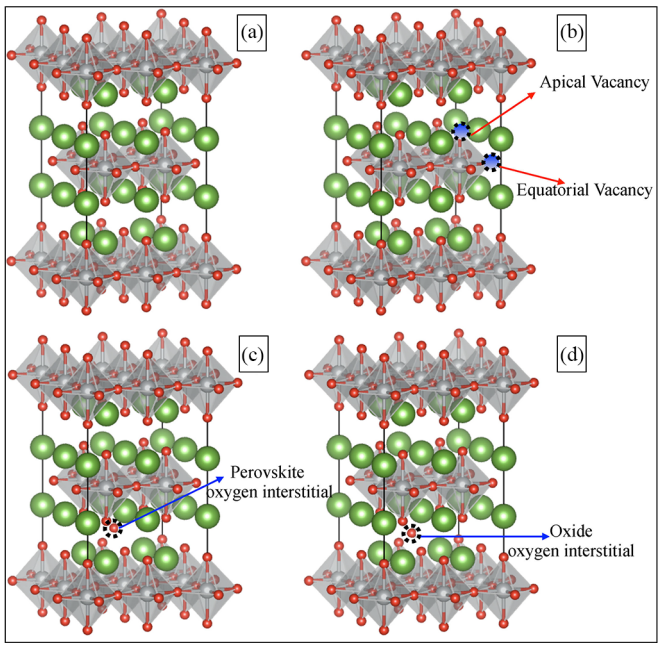

FIG. 1. A 56-atom supercell of La_2NiO_4, showing: (a) the pristine cell, (b) all possible O-vacancy sites, (c) the perovskite interstitial site, and (d) the oxide interstitial site.

essential. However, the very many possibilities of atomic arrangements in $A_{2-x}A'_xB_{1-y}B'_yO_{4\pm\delta}$, even for a particular x, y, and δ, makes it impossible to explore the entire compositional space or to find the ground state with *ab initio* approaches. In this paper, we develop a surrogate model Hamiltonian using cluster expansion (CE) [4] as implemented in the code CELL [5,6], parameterized with density-functional theory (DFT) inputs. CE is one of the most efficient and accurate (in terms of convergence with the training data set size) surrogate models for evaluating relative energies of systems that differ by distribution of atomic species (or defects, such as vacancies) within a well-defined lattice. It takes into account complex many-body interactions between various defects, allowing us to explore the very complex configurational space. Using this model, we have explored the complex configurational space of RP-oxides, taking as an example $La_{2-x}Sr_xNi_{1-y}Fe_yO_{4\pm\delta}$. Figure 1 shows the pristine structure of La_2NiO_4, along with different O-defect sites.

II. METHODS

Spin-polarized DFT [7,8] calculations for all structures with different dopant concentrations are carried out with the all-electron full-potential electronic-structure package FHI-AIMS [9], using numeric atom-centered basis sets. For obtaining a CE model with high predictive power, it is essential to get well-converged DFT energies. A $6\times6\times3$ k-grid mesh and numeric atom-centered basis sets with tight numerical settings as implemented in FHI-AIMS are used to achieve the desired convergence. Each system of $La_{2-x}Sr_xNi_{1-y}Fe_yO_{4\pm\delta}$ is modeled with a supercell of size $2a \times 2a \times c$, where a and c are the lattice vectors parallel and perpendicular to the rock-salt/perovskite layers of the 14-atom conventional unit cell of the K_2NiF_4 type, often referred to as high-temperature tetragonal phase (space-group 139, $I4/mmm$). Therefore, our pristine supercell contains 56 atoms. All the atomic positions as well as the lattice are fully relaxed for each configuration. The choice of exchange-correlation (xc) functional has been carefully validated by comparing the calculated lattice parameters (a_0) and band gaps with experimental ones as well as with the parameters obtained with hybrid functional HSE06 [10]. Table I shows the calculated, experimental lattice parameters, and band gaps for pristine La_2NiO_4 and 50% Sr-doped $LaSrNiO_4$. Based on Table I and considering the balance between accuracy and computational cost, generalized gradient approximation (GGA) with the revised Perdew-Burke-Ernzerhof (RPBE) functional is chosen for the xc treatment. The acceptable performance of a GGA functional for these transition-metal containing oxides is due to the metallic character of their electronic structure, which conceals to some extent the problems in describing localized partially filled d states.

TABLE I. Lattice parameters (a–c), band gaps (e_g), and magnetic moments (m) in pristine La_2NiO_4 and 50% Sr-doped $LaSrNiO_4$: calculated and experimental.

Material	Method	a–c (Å)	e_g(eV)	m
La_2NiO_4	PBE [11]	3.7 3.7 6.9	0.011	1.3
	RPBE [12]	3.75 3.75 6.96	0.049	1.48
	PBE-sol [13]	3.6 3.6 6.95	0.014	0.57
	HSE06 [10]	3.89 3.89 6.82	2.0	2.0
	Experiment [14]	3.8 3.8 6.2	0.2-1.0	1.68
$LaSrNiO_4$	PBE [11]	3.7, 3.7, 6.73	0.019	0.35
	RPBE [12]	3.74, 3.73, 6.79	0.02	0.35
	PBE-sol [13]	3.65, 3.65, 6.64	0.009	0.34
	HSE06 [10]	3.831, 3.831, 6.731	0.44	1.0
	Experiment [15]	3.75, 3.91, 6.425		1.0

One can, in principle, predict the energies of all possible configurations for any x, y, and δ with the CE model. Any arbitrary configuration of the perovskite structure can be represented by a vector $S = (\sigma_1, \sigma_2, ...)$, where the variables σ_i are the occupation variables and can take the value either 1 or 0. When a site i is occupied by one type of atom (e.g., La for the Asite), σ is 1, and when it is occupied with another type of atom (e.g., Sr) σ is 0. Likewise, when the O site is occupied by an O atom, σ is 1, and when there is a vacancy, σ will be 0. For any configuration S, the predicted energy E_s can be expanded in terms of 0, 1, 2,..., n-body clusters $\alpha = \{i, j, ...\}$ as

$$E_s = \sum_\alpha m_\alpha J_\alpha X_\alpha. \quad (1)$$

Here, i and j are the structural sites, J_α are the effective cluster interactions (ECIs), and X_α are the correlations. Correlations are obtained from an average of the so-called cluster functions g_β over all the symmetrically equivalent clusters (denoted by β) to the cluster α. If there are m_α such equivalent clusters, we call the cluster α has a multiplicity m_α. Now these cluster functions $g_{s\beta}$ are defined as the product of the different occupation numbers σ_i (as defined before) for the lattice sites i

belonging to a particular cluster α,

$$g_\beta = \Pi_{i\in\beta}\sigma_i, \tag{2}$$

and X_α are then obtained as

$$X_\alpha = \frac{1}{m_\alpha}\sum_{\beta\equiv\alpha} g_\beta. \tag{3}$$

The ECIs are then obtained by fitting the predicted energies with our calculated DFT energies for initial random structures (viz. training data set). The fitting is performed by minimizing the regularized error function with respect to the ECIs $\mathbf{J} = \{J_\alpha\}$,

$$\mathbf{J}^* = \arg\min_{\mathbf{J}}\left(\frac{1}{N}\sum_{s=1}^{N}[E_{\mathrm{DFT}} - E_s(\mathbf{J})]^2 + A\sum_\alpha |J_\alpha|\right). \tag{4}$$

While the first term of the objective function is the mean-square error in the predicted energies with respect to the calculated energies, the second term is the l_1 regularization term. The purpose of the regularization is to ensure that even if the number of symmetrically distinct clusters exceeds the number of structures in the training set (N), the model can still find the optimal set of ECIs without overfitting. To make sure that overfitting is avoided, the optimal hyperparameter A value is obtained by minimizing leave-one-out cross-validation error (CV),

$$A^* = \arg\min_{A}\left(\frac{1}{N}\sum_{s=1}^{N}[E_{\mathrm{DFT},s} - E_{(s)}(A)]^2\right). \tag{5}$$

Here, $E_{(s)}$ is the predicted value for E_s, which is obtained from a training set excluding the data point s. For more details on the CE modeling, we further refer the reader to Refs. [16,17] and references therein. The energy pool for the CE model is constructed using the formation energies using Eq. (6),

$$\begin{aligned}\Delta E_{\mathrm{form}} = {} & E(\mathrm{La}_{16-x'}\mathrm{Sr}_{x'}\mathrm{Ni}_{8-y'}\mathrm{Fe}_{y'}\mathrm{O}_{32-z'}) \\ & - (16-x')E(\mathrm{La}) - x'E(\mathrm{Sr}) - (8-y')E(\mathrm{Ni}) \\ & - y'E(\mathrm{Fe}) - \frac{(32-z')}{2}E(\mathrm{O}_2).\end{aligned} \tag{6}$$

Using the initial training set, the first iteration of the CE model is carried out. After that the canonical Metropolis Monte Carlo sampling at a fixed temperature 1500 K is performed to find the ground state and metastable structures for each concentration of La/Sr, Ni/Fe and O vacancies. While exploring the configurational space through the Metropolis sampling, a Boltzmann distribution at fixed temperature (1500 K in our case) is generated. The energies of the new structures visited in this procedure are predicted by the CE model. The lowest-energy structures found after 10^6 steps of this sampling for each concentration of Fe, Sr, and O vacancies are further calculated with DFT and are added to the training pool. Then, the CE model is refined with the new training set, and Metropolis sampling is performed again. This process is repeated until no new lower-energy structures are found. Also, the CV must be low enough to get a converged CE model. We found that least absolute shrinkage and selection operator (LASSO) [18] (model is regularized by the sum of absolute values of the weights) works better for treating the complex phase space of the RP phase as compared with linear regression (the most ordinary least-squares method with quadratic regularization). A simple flow chart of the methodology is demonstrated in Fig. 2.

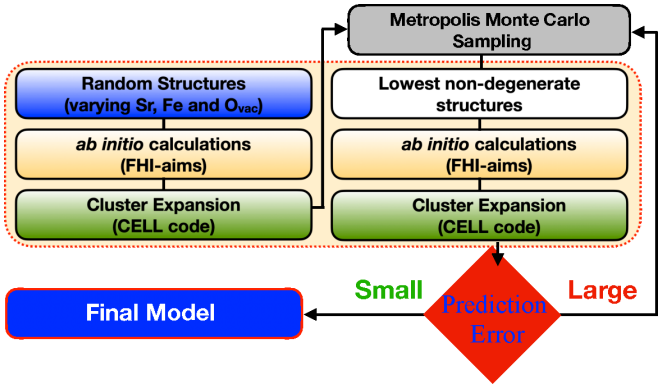

FIG. 2. A flowchart of the methodology used in the present paper, depicting the random structure generation, *ab initio* calculations, and cluster-expansion modeling, followed by Metropolis Monte Carlo sampling for finding lowest nondegenerate structures. The active-learning loop including iterative adding low-energy structures and retraining the model is shown.

In the final iteration of our CE model, we have 251 total structures calculated with RPBE. The distribution of fitting errors per atom and leave-one-out CV error per atom from the final iteration of CE model are shown in Figs. 3(a) and 3(b), respectively. In order to analyze the error distribution within the whole dataset in more detail, we split the dataset into seven groups based on the value of formation energy and calculate the error distribution for each group.

III. RESULTS AND DISCUSSION

By analyzing the low-energy structures, we establish relative energetics of the elemental compositions and distributions, describing structural evolution of the RP oxides with increasing Sr and Fe substitutions. It is shown that the correlation of structural and catalytic activities in terms of electronic density of states is largely dependent on the stable and metastable configurations for a particular composition. To further validate the predictive power of the CE model, we have plotted the model predicted energies along with the calculated energies as a function of Fe concentration for the lowest nondegenerate structures of a particular Sr concentration (x=1.25) in Fig. 4. The O-vacancy formation energies for both apical and equatorial sites are calculated with GGA (RPBE) using the following formula, and the results are shown in SI Table 1 [19],

$$\begin{aligned}\Delta E_{\mathrm{form}} = {} & E(\mathrm{La}_{2-x}\mathrm{Sr}_x\mathrm{NiO}_{4-\delta}) - E(\mathrm{La}_{2-x}\mathrm{Sr}_x\mathrm{NiO}_4) \\ & + \frac{\delta E(\mathrm{O}_2)}{2}\end{aligned} \tag{7}$$

Here, $E(\mathrm{O}_2)$ is the corrected O_2-molecule total energy. The total energy is corrected [20,21] as follows:

$$E(\mathrm{O}_2) = 2E(\mathrm{O}) + E(\mathrm{O}_2)^{\mathrm{bind}}, \tag{8}$$

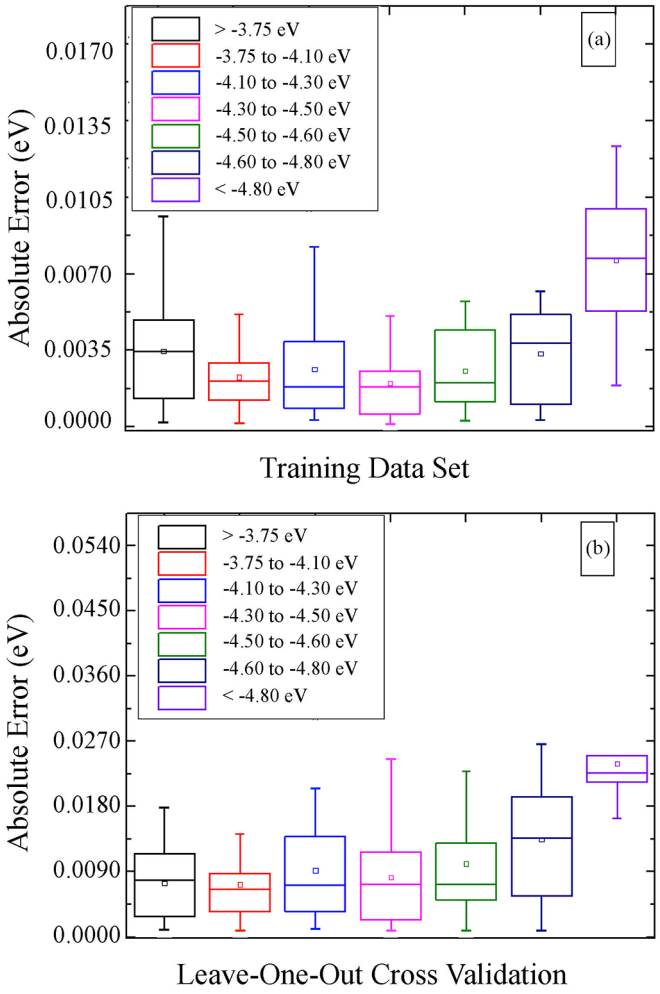

FIG. 3. Box plots of the absolute errors in formation energy [see Eq. (6)] per atom for (a) training set and (b) leave-one-out cross validation for the optimal cluster set. The upper and lower limits of the rectangles represent the 75th and 25th percentiles of the distribution, the internal horizontal lines mark the median (50th percentile), and the upper and lower limits of the error bars indicate the minimum and maximum errors.

where $E(\mathrm{O})$ is the total energy of the O atom, and $E(\mathrm{O_2})^{\mathrm{bind}}$ is the experimental binding energy of $\mathrm{O_2}$ (−5.23 eV [22]). This is to account for the absence of error cancellation when calculating atomic O in the lattice and $\mathrm{O_2}$ molecule in the gas phase with a GGA functional [21]. While only oxygen vacancies are the major defects in ABO_3 perovskites, excess oxygen, or oxygen interstitials are also a major defect in A_2BO_4 RP oxides. For example, in La_2NiO_4, both O_{vac} [23] and O_{int} [24] are reported to be the main oxygen defect species. However, for La_2CoO_4 only oxygen interstitials have been assigned to dominate the defect physics [25]. The interstitial formation energies in pristine La_2NiO_4 for both oxide and perovskite sites as calculated with RPBE functional is given in SI Table 2 [19]. We note that, despite substantial differences in calculated O-defect formation energies, their hierarchy remains unaltered with RPBE as compared to HSE06 functional. Thus, for all the compositions and configurations with O defects, we have used RPBE for our DFT calculations. We find that apical sites in the rock-salt layers are more prone to vacancy formation than the equatorial sites of the perovskite layers in 50% Sr-substituted La_2NiO_4. Substitution of A-site La^{3+} (ionic radius 1.22 Å) with Sr^{2+} (ionic radius 1.31 Å) is a way of acceptor doping in these layered perovskites. This type of doping drives the stoichiometry of the RP phase into oxygen deficient conditions. We found that 50% Sr substitutions at A-site cation site result in increase in interstitial formation energies in La_2NiO_4 and favors vacancy formation, particularly, at the apical site. Since partial Sr substitution at the A-site in La_2NiO_4 typically improves their electrocatalytic activity [1], while constructing our CE model's initial data pool, we have only considered random structures with or without oxygen vacancies, i.e., δ=0.125 or δ=0 are only considered and no interstitials were considered.

Next, we analyze our CE model's predictions by calculating the energy of mixing at the Ni sublattice for a set of Sr concentrations with the following formula:

$$\begin{aligned}\Delta E_{\mathrm{mixing}} = {} & E(\mathrm{La_{2-x}Sr_xNi_{1-y}Fe_yO_{4-z}}) \\ & - yE(\mathrm{La_{2-x}Sr_xFeO_{4-z}}) \\ & - (1-y)E(\mathrm{La_{2-x}Sr_xNiO_{4-z}}). \end{aligned} \quad (9)$$

The energy of mixing for ground-state (or lowest-energy) structures as a function of Fe concentration is plotted in Figs. 5(a)–5(f) for several Sr concentrations with or without O vacancy. We find that, for lower Sr concentrations, the energy gain due to mixing decreases with increasing Fe concentrations. This is because the B-site prefers to retain its +2 charge state with Ni^{2+} sites. However, when Sr^{2+} substitution increases (at La^{3+} sites), the intermediate Fe concentrations get stabilized more by mixing. This observation is interesting since Forslund *et al.* [1] have experimentally observed that $La_{0.5}Sr_{1.5}Fe_{0.3}Ni_{0.7}O_4$ has the highest catalytic activity for OER. Fe is stabilized by electron transfer to the O sublattice, and the highest OER activity is explained by maximizing the number of Ni-O-Fe bridges. Thus, the energy of mixing has an important correlation with the observed activity of this RP material. Moreover, the concentration of Sr plays a crucial role as well. A critical Sr concentration is required to stabilize Fe in these systems. In pure La_2NiO_4, Ni remains in +2 charge state. With increasing Sr, the A-site charge state changes gradually from La^{+3} to Sr^{+2} which facilitates both O-vacancy formation and stabilization of Fe atoms in the lattice. We further note from Figs. 5(c)–5(f) that in presence of O vacancy the intermediate Fe concentrations become more stable, whereas in the pristine systems higher Fe concentrations are

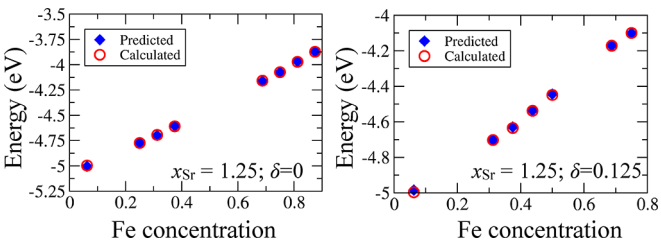

FIG. 4. Comparison of the calculated and CE model predicted formation energies per atom for $La_{0.75}Sr_{1.25}Ni_{1-y}Fe_yO_{4-\delta}$ systems with δ=0, 0.125.

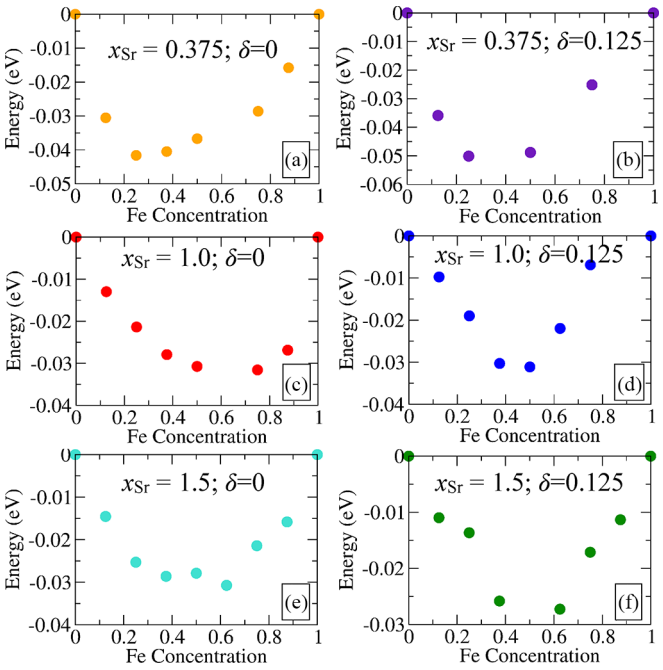

FIG. 5. The energy of mixing as a function of Fe concentration plotted for different Sr and O vacancy concentrations: (a) x_{Sr}=0.375, and δ=0; (b) x_{Sr}=0.375, and δ=0.125; (c) x_{Sr}=1.0, and δ=0; (d) x_{Sr}=1.0, and δ=0.125; (e) x_{Sr}=1.5, and δ=0; (f) x_{Sr}=1.5, and δ=0.125.

favored. This is understandable as Fe drives the *B*-site's charge state towards higher positive number and absence of O atom in the perovskite sublattice hinders the same.

Next, to study the effects of configurational arrangements on electronic structure and, hence, the resultant catalytic and other functional properties of RP oxides, we have analyzed two of the lowest-energy structures for the composition $La_{10}Sr_6Ni_2Fe_6O_{31}$ from our data pool. We find that the apical O-vacancy is more stable than the equatorial one by $\approx$0.3 eV. Also, the vacancy prefers to stay away from either Sr or Fe ions (SI Fig. 1 [19]). However, if we substitute all the transition metal *B* sites with Fe, for example, in $La_6Sr_{12}Fe_8O_{31}$, the vacancy prefers to be in the perovskite layer, i.e., at the equatorial site, and is more stable than the apical one by $\approx$0.3 eV. These structures are shown in SI Fig. 2 [19]. The O atom at the apical site, being at the edge of the layered structure, is much easier to remove compared to the equatorial O atom located inside the perovskite layer. Thus, apical vacancy formation is usually favored. However, the presence of Sr in the perovskite layer can facilitate the vacancy formation as the oxidation state of the *A* site changes from 3+ to 2+. Also, as a general trend, we note from the average stability analysis of the random structures that the O vacancy prefers to be near La sites rather than the substituted Sr sites.

Figures 6(a) and 6(c) show the projected density of states (DOS) of the two configurations of $La_{10}Sr_6Ni_2Fe_6O_{31}$ (see Fig. SI 1 [19]) where the top panel is for equatorial vacancy, and the bottom one is for more stable apical vacancy. We find that a complex interplay of Ni 3*d*-O 2*p*/Fe 3*d*-O 2*p* hybridizations in different configurations of same composition, along with the contributions from La^{3+}/Sr^{2+} plays crucial

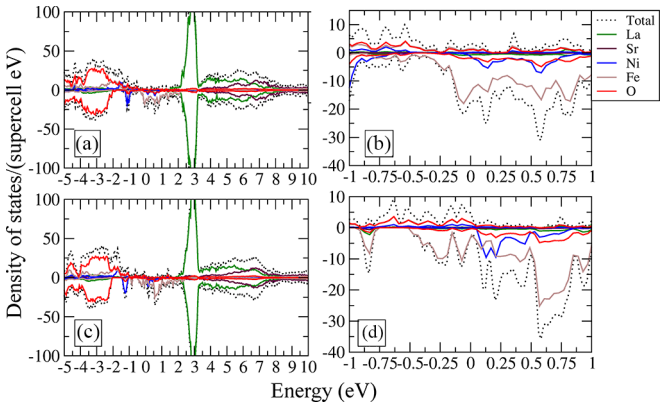

FIG. 6. Projected density of states in a wide energy window [panels (a) ad (c)] and near the Fermi level (zero on the energy axis) [panels (b) and (d) for two different low-energy configurations of $La_{10}Sr_6Ni_2Fe_6O_{31}V_{O_1}$ with equatorial (top) and apical (bottom) O vacancies, respectively (accessible in experiment according to our CE model).

role in determining the electronic structure, and, hence, will largely influence the catalytic activity and other electronic properties of these materials at realistic conditions. In particular, the DOS at the Fermi level for the structure with equatorial vacancy [Fig. 6(b)] is much higher than for structure with the apical one [Fig. 6(d)] due to increased density of Fe states. For the apical vacancy both the *A* site and *B* site substituting Sr and Fe atoms are distributed in different layers, whereas for the equatorial one, only La atoms are neighboring the vacancy site in the lowest-energy configuration. Also, all the *B* sites near the equatorial vacancy are occupied by Fe atoms. This is the reason for the larger contributions from Fe atoms near Fermi energy seen in Fig. 6(b). The equatorial vacancy is surrounded by only La^{3+} sites, whereas the more stable apical one is neighboring both Sr^{2+} and La^{3+} sites, which eases the charge redistribution in the defect-rich RP oxide. Thus, the changes in the near-Fermi level states of different configurations with the same stoichiometry highlight the importance of studying the configurational space in these complex layered oxides. The distribution of Fe/Ni, and, hence, the differences in TM-O bonds' nature, alters the DOS near the Fermi level, which affects the catalytic and other properties directly.

IV. CONCLUSION

In conclusion, we have developed a CE model for RP oxides $La_{2-x}Sr_xNi_{1-y}Fe_yO_{4-\delta}$ based on DFT-RPBE inputs. The model allows us to explore the vast configurational space of these versatile functional materials. Our results show that whereas apical vacancies in the rock-salt layer are more favorable due to lesser steric forces, changes in *A*-site oxidation state due to Sr substitution can facilitate equatorial O-vacancy formation even in the perovskite layers. Furthermore, as the *A*-site charge state gradually changes from La^{+3} to Sr^{+2}, both O-vacancy and *B*-site TM dopants get stabilized in the system. This correlates well with the observed compositional dependence of catalytic activity of these materials in oxygen evolution reaction [1]. Our findings unveil

the significance of configurational re-arrangement effects at realistic conditions on electronic structure of these complex oxides. Thus, before using the electronic-structure features as descriptors of target properties for complex materials, such as RP oxides, the unavoidable effect of atomic rearrangement on these features at experimental conditions must be taken into account.

ACKNOWLEDGMENTS

This work was supported by Russian Science Foundation (RSCF) Grant No. 21-13-00419. D.S. acknowledges the Science and Engineering Research Board (SERB), Govt. of India, Grant No. SRG/2022/001439. We are grateful to K. Stevenson and S. Rigamonti for fruitful discussions.

[1] R. P. Forslund, W. G. Hardin, X. Rong, A. M. Abakumov, D. Filimonov, C. T. Alexander, J. T. Mefford, H. Iyer, A. M. Kolpak, K. P. Johnston *et al.*, Nat. Commun. **9**, 3150 (2018).

[2] J. P. Tidey, E.-P. Liu, Y.-C. Lai, Y.-C. Chuang, W.-T. Chen, L. J. Cane, C. Lester, A. N. D. Petsch, A. Herlihy, A. Simonov *et al.*, Sci. Rep. **12**, 14343 (2022).

[3] W. Xie, Y.-L. Lee, Y. Shao-Horn, and D. Morgan, J. Phys. Chem. Lett. **7**, 1939 (2016).

[4] J. Sanchez, F. Ducastelle, and D. Gratias, Physica A **128**, 334 (1984).

[5] S. Rigamonti, M. Troppenz, and C. Draxl (unpublished).

[6] Cell documentation, https://sol.physik.hu-berlin.de/cell.

[7] P. Hohenberg and W. Kohn, Phys. Rev. **136**, B864 (1964).

[8] W. Kohn and L. J. Sham, Phys. Rev. **140**, A1133 (1965).

[9] V. Blum, R. Gehrke, F. Hanke, P. Havu, V. Havu, X. Ren, K. Reuter, and M. Scheffler, Comput. Phys. Commun. **180**, 2175 (2009).

[10] A. V. Krukau, O. A. Vydrov, A. F. Izmaylov, and G. E. Scuseria, J. Chem. Phys. **125**, 224106 (2006).

[11] J. P. Perdew, K. Burke, and M. Ernzerhof, Phys. Rev. Lett. **77**, 3865 (1996).

[12] Y. Zhang and W. Yang, Phys. Rev. Lett. **80**, 890 (1998).

[13] J. P. Perdew, A. Ruzsinszky, G. I. Csonka, O. A. Vydrov, G. E. Scuseria, L. A. Constantin, X. Zhou, and K. Burke, Phys. Rev. Lett. **100**, 136406 (2008).

[14] X. Batlle, X. Obradors, and B. Martnez, Phys. Rev. B **45**, 2830 (1992).

[15] Z. H. and Z. R., J. Serb. Chem. Soc **71**, 1049 (2006).

[16] M. Troppenz, S. Rigamonti, and C. Draxl, Chem. Mater. **29**, 2414 (2017).

[17] Z.-K. Han, D. Sarker, M. Troppenz, S. Rigamonti, C. Draxl, W. A. Saidi, and S. V. Levchenko, J. Appl. Phys. **128**, 145302 (2020).

[18] R. Tibshirani, J. R. Statist. Soc.: Ser. B (Methodological) **58**, 267 (1996).

[19] See Supplemental Material at http://link.aps.org/supplemental/10.1103/PhysRevMaterials.7.055802 for the O-vacancy formation energies, the O-interstitial formation energies calculated with RPBE, lowest-energy configurations for the composition $La_{10}Sr_6Ni_2Fe_6O_{31}$, and lowest-energy configurations for the composition $La_6Sr_{12}Fe_8O_{31}$.

[20] W.-X. Li, C. Stampfl, and M. Scheffler, Phys. Rev. B **65**, 075407 (2002).

[21] K. Reuter and M. Scheffler, Phys. Rev. B **65**, 035406 (2001).

[22] M. W. Chase Jr., *NIST-JANAF Themochemical Tables*, 4th ed., J. Phys. Chem. Ref. Data, Monograph **9**, 1 (1998).

[23] A. Cleave, J. Kilner, S. Skinner, S. Murphy, and R. Grimes, Solid State Ionics **179**, 823 (2008).

[24] C. Frayret, A. Villesuzanne, and M. Pouchard, Chem. Mater. **17**, 6538 (2005).

[25] T. Nakamura, K. Yashiro, K. Sato, and J. Mizusaki, Solid State Ionics **180**, 368 (2009).